INVESTIGATING TILTROTOR FORMATION FLIGHT VIA $^1/_{48}$-SCALE WIND TUNNEL EXPERIMENT

Ethan Romander
Mark Betzina
Flight Vehicle Research and Technology Division
NASA Ames Research Center
Moffett Field, CA
ethan.a.romander@nasa.gov
mark.d.betzina@nasa.gov

Mark Silva
Advanced Aerodynamics Branch
NAVAIR Air Vehicle Department
Patuxent River, MD
mark.silva@navy.mil

Alan Wadcock
Fluid Mechanics Institute
Boulder Creek, CA
wadcock@merlin.arc.nasa.gov

Gloria Yamauchi
Aeronautics Projects Office
NASA Ames Research Center
Moffett Field, CA
gloria.k.yamauchi@nasa.gov

Abstract

This paper describes two small-scale wind tunnel tests conducted in the Army 7- by 10-Foot Wind Tunnel at NASA Ames Research Center. These tests featured two $^1/_{48}$-scale V-22 models that were operated in a variety of simulated flight conditions including climb, descent, and level flight at various flight speeds and spatial separations. Forces and moments experienced by the trail aircraft were used to deduce the influence of the lead aircraft on the trail aircraft. Particle Image Velocimetry (PIV) data were collected to relate these forces and moments to features in the lead aircraft wake. In general, the roll moment on the trail aircraft is shown to be maximum when the aircraft are laterally offset by a full wingspan and the trail aircraft is vertically positioned so as to be in the wake of the lead aircraft. Furthermore, the roll moment is maximal when operating near 50 knots full-scale flight speed. Because the interaction persists far downstream and the vertical position of the wake is dependent on descent angle and flight speed, lateral separation has been determined to be the best means of avoiding adverse interactions between aircraft.

Presented at the American Helicopter Society 62nd Annual Forum, Phoenix, AZ, May 9–11, 2006.

Report Documentation Page

Form Approved
OMB No. 0704-0188

1. REPORT DATE	2. REPORT TYPE	3. DATES COVERED
MAY 2006		**00-00-2006 to 00-00-2006**

4. TITLE AND SUBTITLE	5a. CONTRACT NUMBER
Investigating Tiltrotor Formation Flight Via 1/48-Scale Wind Tunnel Experiment	5b. GRANT NUMBER
	5c. PROGRAM ELEMENT NUMBER
6. AUTHOR(S)	5d. PROJECT NUMBER
	5e. TASK NUMBER
	5f. WORK UNIT NUMBER
7. PERFORMING ORGANIZATION NAME(S) AND ADDRESS(ES) **US Army Aviation and Missile Command,Army/NASA Rotorcraft Division,Army Aeroflightdynamics Directorate (AMRDEC),Moffett Field,CA,94035**	8. PERFORMING ORGANIZATION REPORT NUMBER
9. SPONSORING/MONITORING AGENCY NAME(S) AND ADDRESS(ES)	10. SPONSOR/MONITOR'S ACRONYM(S)
	11. SPONSOR/MONITOR'S REPORT NUMBER(S)

12. DISTRIBUTION/AVAILABILITY STATEMENT
Approved for public release; distribution unlimited

13. SUPPLEMENTARY NOTES

14. ABSTRACT
see report

15. SUBJECT TERMS

16. SECURITY CLASSIFICATION OF:			17. LIMITATION OF ABSTRACT	18. NUMBER OF PAGES	19a. NAME OF RESPONSIBLE PERSON
a. REPORT **unclassified**	b. ABSTRACT **unclassified**	c. THIS PAGE **unclassified**	**Same as Report (SAR)**	**19**	

Notation

A	Total rotor disk area, $2\pi R^2$
C_T	Rotor thrust coefficient, $\frac{T}{\rho(\Omega R)^2 A}$
D	Rotor diameter
DCP	Differential Collective Pitch, deg
PIV	Particle Image Velocimetry
R	Rotor radius
s	Aircraft semispan length
T	Total rotor thrust
V_∞	Freestream velocity
V_h	Ideal hover induced velocity, $\sqrt{\frac{T}{2\rho A}}$
X, Y, Z	Inertial axis basis vectors
α_f	Fuselage angle of attack, deg
β	Sideslip angle, deg
γ	Flight path angle, deg
θ	Fuselage pitch angle in-flight, deg
Ω	Rotor angular velocity
ω	Vorticity, $^1/_{\text{sec}}$
ρ	Freestream density
χ, υ, ζ	Wind axis basis vectors

Introduction

Military aircraft fly in close formations. Likewise, the ability to operate in loose formation allows civilian aircraft to maximize the throughput at a base of operations. Unfortunately, the revolutionary nature of tiltrotor aircraft produces some uncertainty about the safety of formation flight, particularly at low speeds. The military has invested some effort in full-scale flight tests to investigate the performance of the V-22 Osprey in formation flight, but has been unable to thoroughly prosecute all possible configurations. Additional fundamental research is required in order to help guide military flight test research programs and to assist in the development of analytical models to further the understanding of tiltrotor aircraft wakes.

Substantial effort has already been expended attempting to understand the mutual interaction between tiltrotor aircraft [Refs. 1-2]. Additional work has been directed into understanding the complex environment of simultaneous aircraft operations aboard seagoing vessels [Refs. 3-4]. This paper expands upon this base of research by considering additional flight conditions and providing detailed measurements of the combined wake systems for use in development of analytical models. These goals were met by a series of small-scale wind tunnel tests conducted in the Army 7- by 10-Foot Wind Tunnel at NASA Ames Research Center.

The first test was conducted from June to October 2004 and focused on low speed operations in VTOL mode. Consequently, this test only considered a 90 degree nacelle angle (i.e., a horizontal tip-path-plane) and 73 deg of flap deflection. The remaining test parameters for the first test are listed in Table 1.

Table 1. Simulated parameters for first wind tunnel test

Flight Speed:	20 to 50 knots
Thrust Coefficient:	0.009 to 0.018 (nominally 0.014, or 47,500 lb gross weight at sea level)
Rate of Climb:	-2500 $^{\text{ft}}/_{\text{min}}$ (descent) to $+1000$ $^{\text{ft}}/_{\text{min}}$ (climb)
Flight Path Angle:	11.38 deg to -29.56 deg
Sideslip Angle:	0 deg and -15 deg

The second test was performed from August to December 2005. This test sought to expand the test matrix of the first test by exploring formation flight at flight speeds of up to 110 knots. In order to maintain fidelity with operational tiltrotor aircraft, the models were operated at nacelle angles of 60 deg to 85 deg full-scale and a wing flap deflection of 40 deg. Unlike the first test, this iteration did not investigate sideslip or weight variations. The test matrix is listed in Table 2. In addition to the higher flight speeds, the second test also added Particle Image Velocimetry (PIV) measurements in an attempt to directly measure the wake influencing the trail aircraft.

Table 2. Simulated parameters for second wind tunnel test

Flight Speed:	50 to 110 knots
Aircraft Gross Weight:	47,500 lb
Rate of Climb:	-1000, 0, +1000 $^{\text{ft}}/_{\text{min}}$
Flight Path Angle:	11.39 deg to -11.39 deg
Sideslip Angle:	0 deg

Approach

$^1/_{48}$-Scale Tiltrotor Models

The experimental apparatus for both tests was very similar. Both tests used the same models, one of which is pictured in Fig. 1. The models are designed to nominally resemble $^1/_{48}$-scale V-22 aircraft. Much of the model hardware consists of commercially available remote control model helicopter components with custom elements designed to integrate these components into a functional

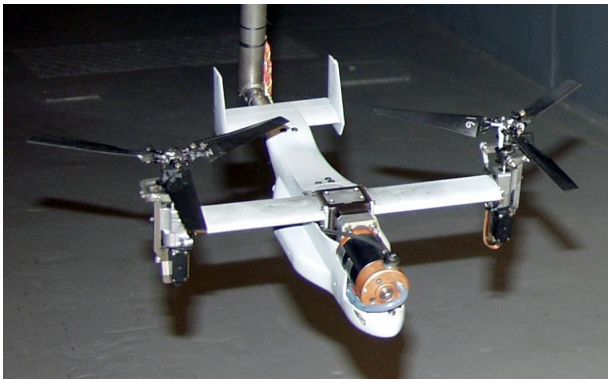

Figure 1. $1/48$-scale V-22 model.

model. The initial design of these models is described in Ref. 5.

The wings and wing flaps were constructed using a selective laser sintering process and are scale replicas of V-22 hardware. The automatic flap control system for the V-22 mandates a flap setting of 73 deg for flight speeds up to 45 knots. This was the only flap setting used at simulated flight speeds below 50 knots. For flight speeds above 50 knots, an alternate flap deflection of 40 deg was used. This setting is within 3 deg of the settings that would be selected by the automatic flap system aboard the V-22 for the simulated configurations at 80 and 110 knots. Figure 2(a) is a detail photo of the wing and flap system. Note that the flap follower and gap are appropriately represented.

Due to the low Reynolds number and difficulty matching V-22 geometry at this small scale, model airframe lift coefficient was substantially lower than would be expected from the V-22 under equivalent conditions. For this reason, the wings were fitted with trip strips to better model the lift-curve slope of the full-scale V-22. The selected trip strip design is shown in Fig. 2(b). The strips had a serrated leading edge, a thickness of 0.013 inches, and were located at approximately 5% chord. Because airframe lift is insignificant at low speeds, these trip strips were only in place when simulating flight at or above 50 knots.

The rotor diameter and twist distribution were scaled directly from V-22 specifications. Due to power limitations of the model motor, the rotor was operated at $1/3$ V-22 tip speed. Tunnel velocity was set to $1/3$ of the simulated velocity so that the model rotor advance ratio matched full-scale advance ratio. The limited tip speed and small scale resulted in a model Reynolds number that was just $1/144$ the full-scale Reynolds number. In order to match thrust coefficients with the full-scale V-22, the model rotors used low Reynolds number airfoils and the chord of each blade was increased by 38% compared to scaled V-22 dimensions.

The rotor hub allowed only lead-lag motion of the blades and provided control solely of collective pitch. The model control system was capable of controlling the two rotors independently and therefore could use differential collective pitch—a collective increase on one rotor coupled with an equal collective decrease on the other—to control the model roll moment.

Each model was mounted on an internal six component balance that provided measurement of total aircraft aerodynamic forces and moments.

Test Conditions

The goal of these tests was to simulate aircraft operation in a variety of realistic flight conditions. The conditions were directly derived from ongoing Navy V-22 flight testing and involved climbing and descending flight at various flight speeds.

In studying wake interaction between tiltrotor aircraft, it is most important to properly simulate the rotor thrust coefficient, advance ratio, and tip-path-plane angle-of-attack. For this study, these parameters were set using two approaches. At simulated speeds up to 50 knots, the model nacelles were fixed at 90 deg and the rotor tip-path-plane was assumed to be horizontal. This is a reasonable approximation of V-22 performance in this speed regime because airframe drag is low. At speeds above 50 knots this assumption is no longer valid. The V-22 nacelles typically are tilted forward commensurate with flight speed, and the tip-path-plane orientation is dependent on airframe pitch and blade flapping. At these higher speeds, the model was configured as described below.

Simulations were run using CASTLE, the Controls Analysis and Simulation Test Loop Environment. This version of CASTLE employed the Bell Helicopter Generic Tiltrotor (GTR) math model version 0201 and an implementation of the V-22 controls laws version 12.1.1. These simulations yielded a unique tip path plane angle-of-attack, fuselage angle-of-attack, and nacelle angle for each speed and descent rate combination investigated. The tip-path-plane angles resulting from these simulations represent the superposition of nacelle tilt, blade flapping, and fuselage pitch at each condition. However, the model blades were incapable of flapping, requiring that the tip-path-plane angle-of-attack on the model be set by the nacelle angle and fuselage angle-of-attack alone. For each speed, the model nacelle angle was altered slightly from the CASTLE prediction to account for the average blade flapping at all descent rates. The resulting model nacelle angles are given in Table 3. Deviations from this average tip-path-plane angle at each descent rate were accounted for by slight adjustments to the

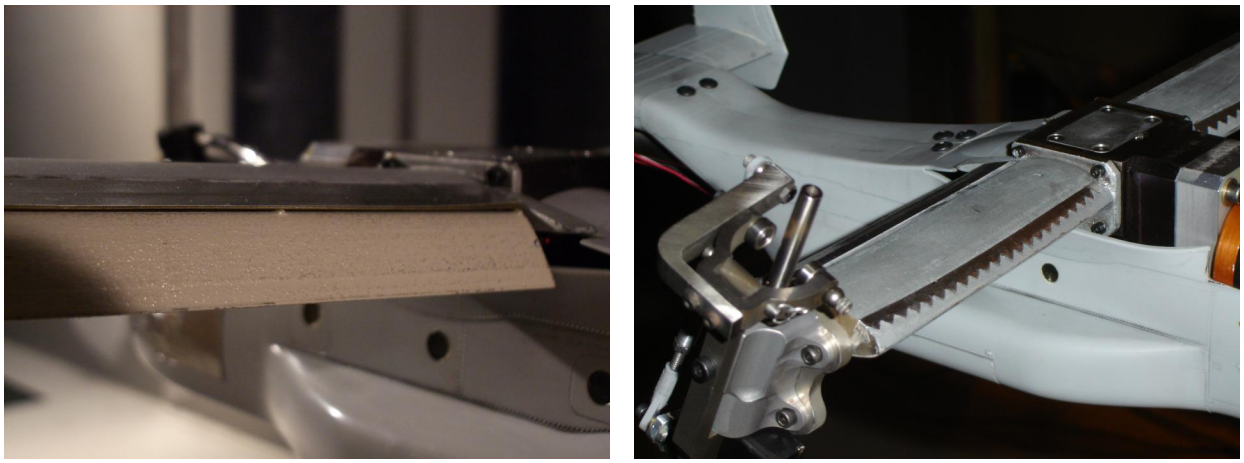

(a) Flap follower and gap (b) Wing trip strip

Figure 2. Model wing detail photos

Table 3. Model nacelle angle settings

Full-scale speed, knots	Full-scale nacelle angle, deg.	Model nacelle angle, deg.
<50	90	90
50	85	86
65	85	86
80	75	77
110	60	64

fuselage angle-of-attack. Thus, the rotor tip-path-plane angle-of-attack was matched to CASTLE predictions for all test conditions at the price of small departures from CASTLE predicted nacelle angle and fuselage angle-of-attack.

In the course of this text, model location will always be defined by the model reference point. The model reference point is defined to be the midpoint of the line connecting the centers of the two rotor disks.

A brief introduction to the axis systems involved is necessary in order to fully understand the present test configuration. The three axis systems are briefly illustrated in Fig. 3.

The aircraft body axis system is defined by the fuselage, with principal axes being out the nose, out the right wing, and down. It is in the body axis system that all forces and moments were measured by the model balance.

In flight, pilots operate their vehicles relative to a separate, quasi-inertial axis system defined by the vectors X, Y, and Z. Projection of the longitudinal and lateral body

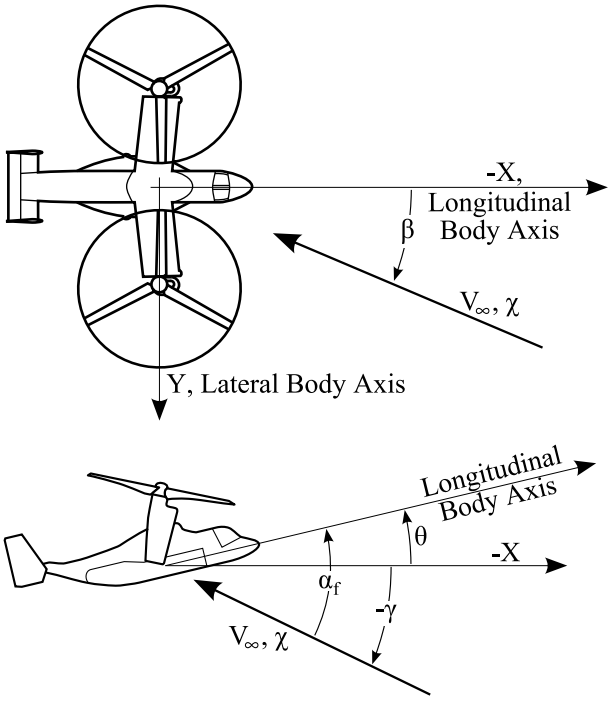

Figure 3. Axis systems for an in-flight V-22

axis vectors onto the local horizontal plane define the inertial $-$X and Y axes respectively. The inertial axis system yaws with the aircraft but does not pitch or roll. The angle between the longitudinal body axis and the $-$X inertial axis vector is commonly called the pitch angle, θ. This axis system is particularly significant because a pilot considers his position relative to neighboring aircraft by reference to the inertial axis system. This was therefore the axis system used to measure model separation.

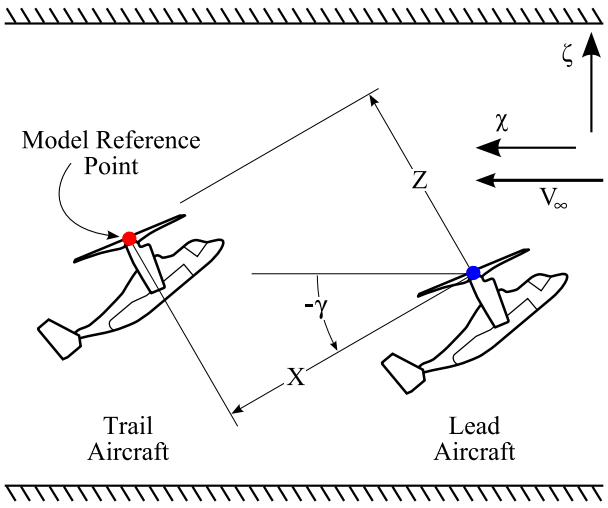

Figure 4. Model orientation for descending flight in wind tunnel

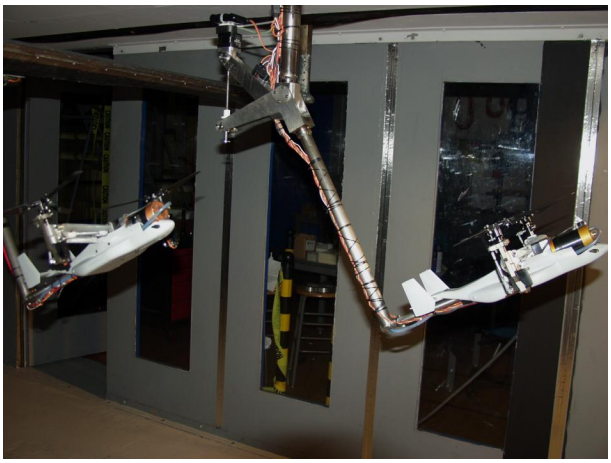

Figure 5. Lead aircraft model mounted to fixed strut (right), trail aircraft mounted to three axis traverse (left)

A third axis system, called the wind axis system, exists in a wind tunnel and is defined by the vectors χ, υ, and ζ. The χ vector is in the streamwise direction, parallel to the freestream velocity vector. The remaining vectors are chosen to define the lateral and vertical directions relative to the tunnel installation. The wind axis system and the inertial axis system are related by two fundamental angles. First, the formation flight path angle, γ, is the angle between the χ axis and the $-$X axis in the X-Z plane. The second fundamental angle is the formation sideslip angle, β; the angle between the χ axis and the $-$X axis measured in the X-Y plane. Together, these two angles define the direction of flight for the formation in the inertial axis system.

In flight, the freestream vector rotates in the inertial axis system as the formation changes its flight path. However, because the freestream vector direction—and therefore the wind axis system—is fixed in the wind tunnel, sideslip, climbing, and descending flight are simulated by rotating the inertial axis relative to the wind axis by the flight path and sideslip angles. This configuration is illustrated in Fig. 4. For convenience, the origin of the inertial axis system is taken to be the reference point of the lead aircraft. Note that although the inertial axis origin is fixed to the lead model, it is inclined by the flight path angle and not the fuselage angle of attack. The inertial axis and aircraft body axis will align only when the fuselage pitch angle is zero.

Force And Moment Data Acquisition

A single model, representing the lead aircraft in the formation, was mounted to a fixed strut that provided only model pitch and yaw motions. A second model, representing the trail aircraft, was mounted on a three-axis traverse via an identical strut which provided the same pitch and yaw motions. The model support struts were always configured to place the two models at the same pitch and yaw angles—as would be the case for aircraft flying in formation. The two models are shown pitched upward for a descending flight condition in Fig. 5.

At the start of a data collection run, the models were initially trimmed to a given lift coefficient while far apart and free from any mutual influence. The models were then brought together and the trail model traversed through a plane of constant X or Y in the inertial axis system. During this motion, the thrust coefficient of the lead model was held in trim by varying the collective pitch. Lead model roll was likewise neutralized using differential collective pitch (DCP). Conversely, the collective pitch and DCP of the trail model were held constant, thereby permitting thrust coefficient and roll moment to vary with rotor inflow. At a series of points in the plane of interest, the roll moment of the trail model was measured and used to infer the effect of the lead aircraft on the trail aircraft.

A sample data collection matrix is given in Fig. 6. This figure is from the perspective of an observer standing on the X axis, looking at the formation from behind. The lead model is located at the top left in the figure and remains stationary. The points in the figure represent locations downwind of the lead aircraft and in a plane of constant X. It is at these locations that the trail model would pause to collect force and moment data during a survey. Note that at all times, model position is measured in the inertial reference frame and is defined by the model reference point, highlighted in Figs. 4 and 6. Data points were clustered in regions where the interaction between

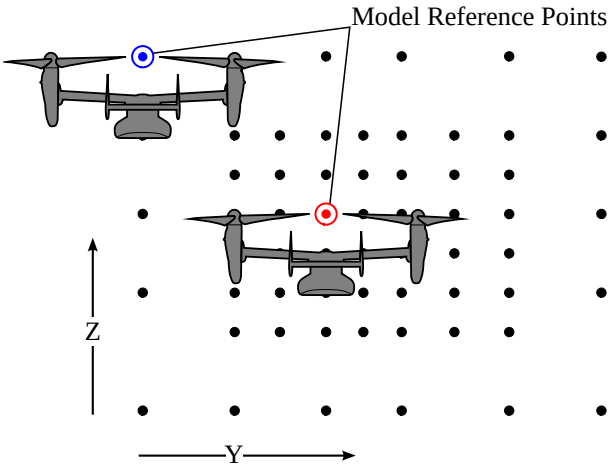

Figure 6. Sample data collection matrix viewed from behind formation. Highlighted points indicate model reference points.

the two models was expected to be maximal.

The rotor thrust coefficient set for the lead aircraft and nominally set for the trail aircraft was determined from CASTLE simulations and was intended to be representative of the rotor thrust on flight hardware. Assuring this similarity was difficult because the models did not supply separate measurements of rotor thrust and airframe lift but rather measured total aircraft lift:

$$\text{total lift} = \text{rotor thrust} + \text{airframe lift}$$

At flight speeds below 50 knots, airframe contributions to total lift are negligible, which means that total aircraft lift and rotor thrust are approximately equal. However, higher flight speeds result in significant contributions to lift from the airframe. Lift contributions from the airframe needed to be accounted for so that setting the trim condition using the total model lift yielded a rotor thrust comparable to the full-scale aircraft. To this end, a series of tare runs were executed in which the model rotors were removed and supported from above by a separate apparatus. This apparatus positioned and operated the rotors identically to the model but was mechanically separate (see Fig. 7). In this configuration, separate measurements of rotor and airframe contributions to model lift were possible. Thus airframe lift was determined for all descent rates and speeds above 50 knots. This airframe lift was subtracted from the total model lift, as measured by the balance, to obtain the proper rotor thrust when adjusting model trim.

The force and moment data collected during a single survey were normalized by reference data taken at the start and end of each run to account for experimental drift during a run. The roll moment data were then converted

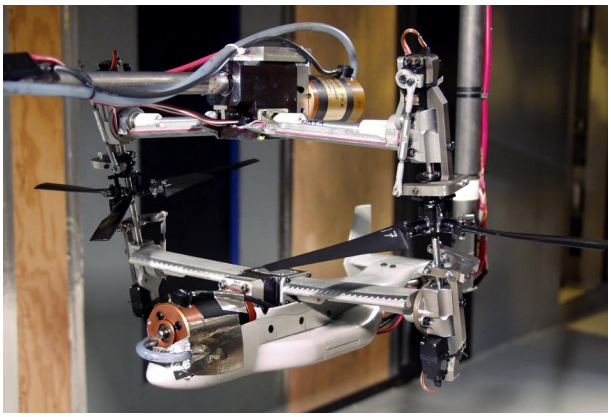

Figure 7. Model airframe lift calibration configuration

into the equivalent differential collective pitch (DCP) required to neutralize the roll moment. One deg of DCP is equivalent to a 1 deg increase in collective pitch on one rotor *and* a 1 deg decrease on the other rotor. The sign convention for DCP is the same as it is for roll moment, namely positive for a DCP that results in right wing down roll moment. This conversion was performed using data from a series of tare runs that carefully calibrated the relationship between DCP and model roll moment at each speed.

Differential collective pitch is used as the primary metric for the interaction between aircraft because it provides better comparison with full-scale aircraft performance. Roll moment is a function of rotor solidity whereas DCP is not. Results cast in terms of DCP are therefore expected to be valid despite the difference in solidity between the model and the full-scale aircraft.

PIV Data Acquisition

It is important to note that the aforementioned procedure for measuring trail aircraft roll moment is not intended to provide a direct measurement of the lead aircraft wake. Rather, it is intended to measure the effect of the lead aircraft wake *integrated over the trail aircraft*. This distinction is important because it is possible for two vastly different wake systems to induce the same roll moment if they interact with the trail aircraft in different ways. In order to fully understand the origin of the force and moment measurements, it is necessary to directly measure the wake incident on the trail aircraft.

One technique commonly used in wind tunnel testing is Particle Image Velocimetry (PIV). PIV provides a simultaneous measurement of all three velocity components in a selected plane. This is accomplished using two separate cameras to track individual seed particles as they pass through a laser light sheet. This simultaneous, planar measurement is ideal for measuring aircraft wakes.

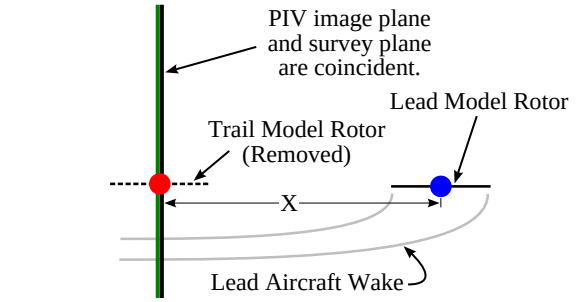

(a) Level flight

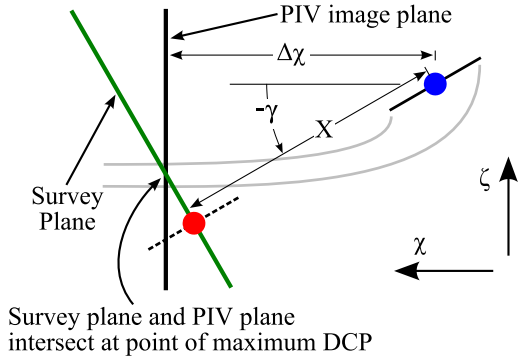

(b) Descending flight

Figure 8. The relationship between the model, the PIV laser sheet, and the force and moment survey plane.

The wake encountered by the trail aircraft in a formation is measured by placing a single model upstream of the PIV laser sheet. The force and moment data in conjunction with PIV data taken at the same flight condition permits correlation between wake structure and the corresponding forces induced on a trail aircraft.

The configuration for PIV data acquisition is illustrated in Fig. 8. The trail model was removed from the tunnel, and a vertical laser sheet was formed in the position formerly occupied by the trail model rotors. Figure 8(a) represents a level-flight PIV configuration. In this configuration, the PIV laser light sheet is coincident with the survey plane in which level-flight force and moment measurements were made. Thus PIV measurements reflect the exact same wake structure that was integrated and recorded as force and moment data for a given level-flight condition.

As shown in Fig. 8(b), PIV data acquisition was more complicated when simulating climbing or descending flight. To achieve these flight conditions, the lead model was rotated about its reference point by the flight path angle, γ. Recall that this rotation of the inertial reference frame also rotated the survey plane in which force and moment measurements were conducted. The laser sheet, however, was fixed in a vertical orientation, preventing PIV measurement in the rotated survey plane. Because the flight path angles were kept small ($|\gamma| \leq 11.39$ deg) during PIV measurements and because streamwise gradients were also small, this misalignment is not believed to introduce significant error into the velocity field measurements. However, in order to minimize any measurement error near the location of peak DCP, the distance between the model and the laser sheet, $\Delta\chi$, was chosen such that the laser sheet intersected the survey plane at the location where peak DCP was measured.

Results and Discussion

Representative Measurements

Figure 9 shows reduced data typical for this experiment. The data in Fig. 9 represents aircraft operating at 80 knots in a 1000 $^{\text{ft}}/_{\text{min}}$ descent with nacelles at 75 deg and at a gross weight of 47,500 lb. The DCP data in Fig. 9(a) represents the differential collective pitch required to trim the roll moment to zero. The DCP data were taken in a plane of varying Y and Z with X held constant such that $^{\text{X}}/_{\text{D}} = 2.818$. This value of X is indicative of a 50-foot separation at full-scale between the nose of the trail aircraft and the tail of the lead aircraft.

In Fig. 9, as well as throughout this paper, the lead aircraft was stationary, with its reference point at the plot origin. The abscissa in Fig. 9(a) represent lateral offsets between the trail aircraft reference point and the lead aircraft centerline. These offsets are nondimensionalized by the semispan distance, $^1/_2$ the distance between rotor hubs. Similarly, the ordinates in Fig. 9(a) represent vertical distances between the trail aircraft reference point and the lead aircraft rotor plane, also nondimensionalized by the semispan distance.

The DCP data exhibit excellent antisymmetry about the lead aircraft centerline: There exists a strong region of positive DCP approximately two semispans to the right of the lead aircraft. This region of positive DCP has a corresponding DCP peak of equal magnitude but opposite sign approximately two semispans to the left of the lead aircraft. Because of this symmetry, the remaining data for this study were acquired only for $^{\text{Y}}/_{\text{s}} \geq 0$.

The positive DCP required near $^{\text{Y}}/_{\text{s}} = 2$ is necessary to offset a negative (left wing down) rolling moment. Furthermore, observe that although much of the rest of the right half-plane reflects a slightly positive required DCP, there is a small region outboard of $^{\text{Y}}/_{\text{s}} = 3$ in which a slightly negative DCP is required of the trail aircraft.

The plot of required DCP gives an indication of the nature and magnitude of the interaction between these

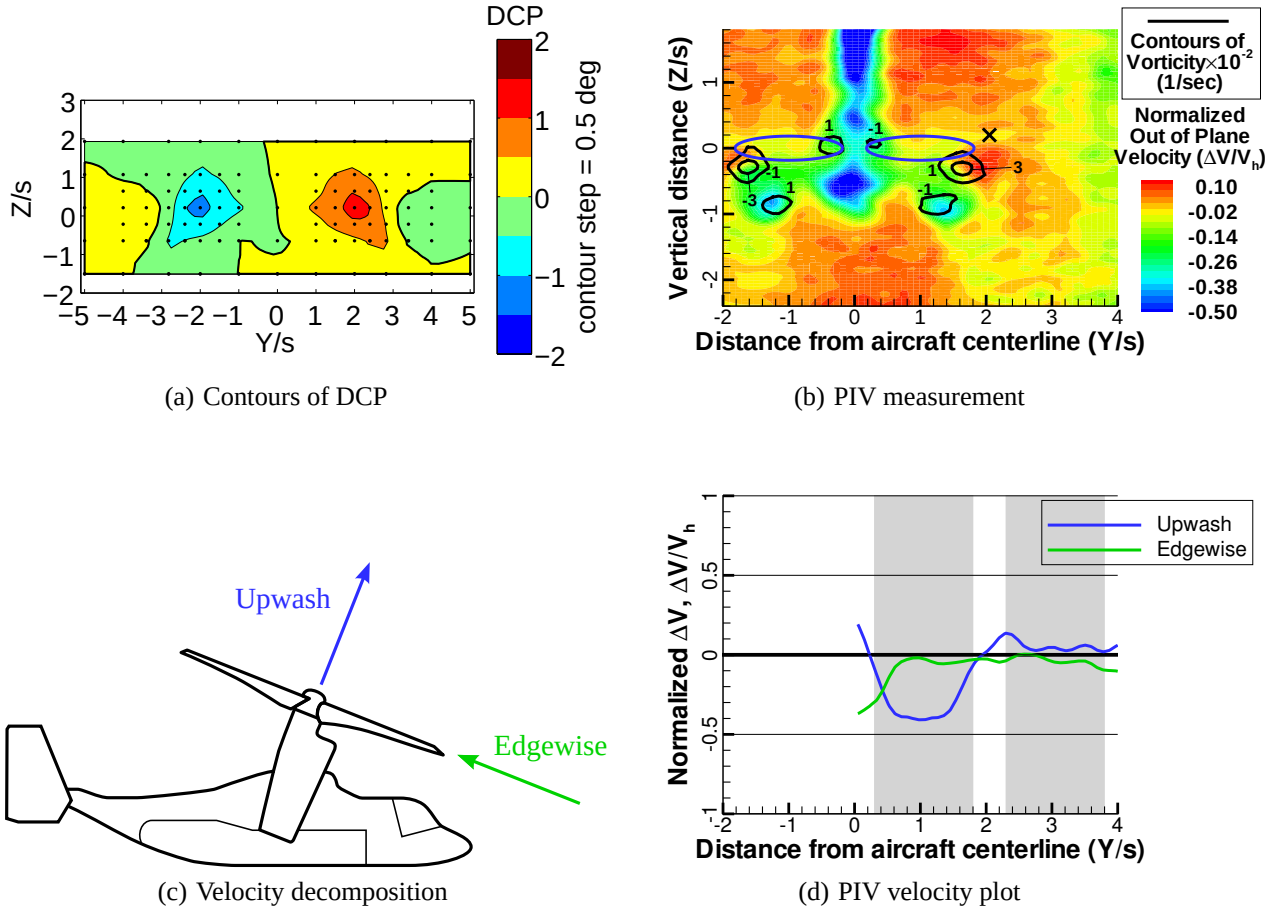

(a) Contours of DCP

(b) PIV measurement

(c) Velocity decomposition

(d) PIV velocity plot

Figure 9. Formation flight at 80 knots full-scale, 1000 $^{ft}/_{min}$ descent, $C_T = 0.010$, $^{X}/_{D} = 2.818$

aircraft in formation, but it does little to relate these interactions to specific wake features. This task will be served by PIV measurements.

Figure 9(b) shows the PIV measurement for the same flight condition. The lead aircraft rotor disks are represented by the blue ellipses centered about the origin. The color contours indicate change in velocity (relative to the freestream) normal to the laser sheet, normalized by the hover induced velocity, V_h. Normalization of PIV velocities by V_h removes sensitivity to differences in rotor thrust when comparing different flight conditions. The region of velocity deficit just beneath the rotors results from the aircraft fuselage (at $^{Y}/_{s} = 0$), wings (extending from the centerline to $^{Y}/_{s} = \pm 1$), and nacelles (located at $^{Y}/_{s} = \pm 1$). The prominent velocity deficit extending upward from the rotor plane along the aircraft centerline results from the model support strut.

To provide a concise representation of the in-plane rotor wake, black lines trace contours of constant out-of-plane vorticity in Fig. 9(b). At the center of a closed contour of vorticity lies a vortex core. It is possible to identify the two wake super vortices located just below the rotor disks at $^{Y}/_{s} = \pm 1.6$. The starboard vortex has a peak vorticity of 0.03/sec indicating strong, counterclockwise flow around its core. The corresponding vortex on the port side of the aircraft is equal in strength but opposite in rotation. In addition to the two super vortices, there are four other, weaker vortices: two just above and near the inboard edge of the rotor disks, and two just beneath and inboard of the wake super vortices.

Lastly, a small "×" in Fig. 9(b) identifies the location of peak positive DCP in Fig. 9(a).

Examining the PIV data in Fig. 9(b), the cause of peak positive DCP becomes clear. When at the point of peak positive DCP, the trail aircraft is nearly centered on the starboard super vortex in the wake of the lead aircraft. The counterclockwise rotation of this super vortex induces downwash on the trail aircraft left rotor and upwash on the right rotor. The resulting thrust imbalance, coupled with a similar effect on the airframe itself, results in a net negative roll moment induced on the trail aircraft. This negative roll moment is neutralized by the

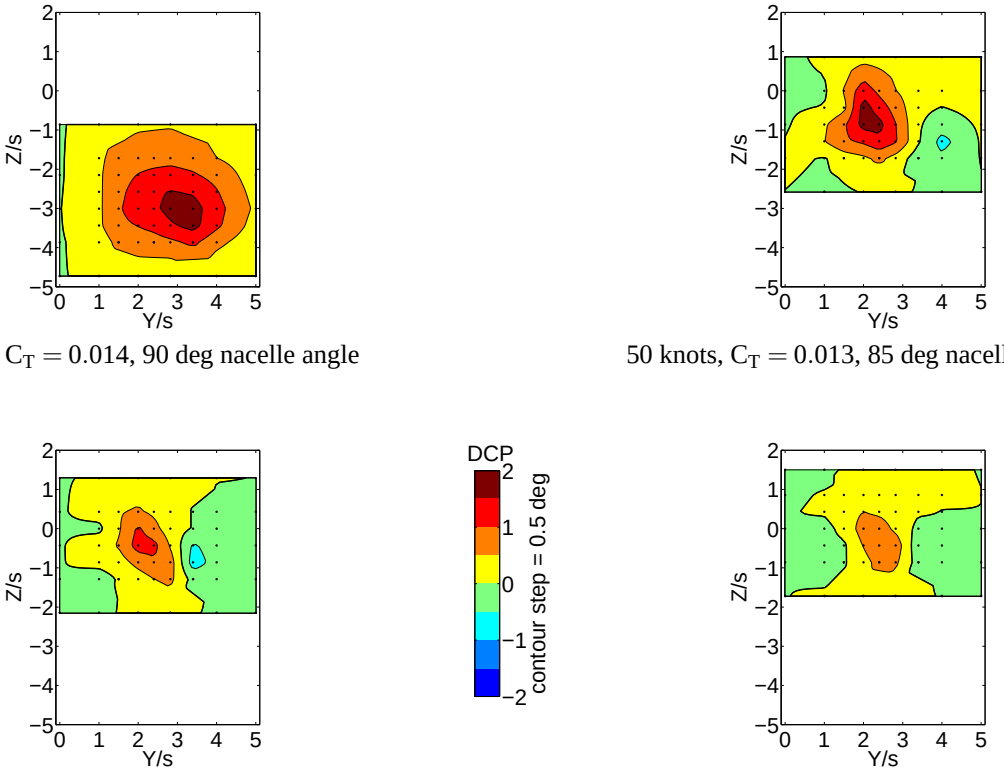

20 knots, $C_T = 0.014$, 90 deg nacelle angle

50 knots, $C_T = 0.013$, 85 deg nacelle angle

80 knots, $C_T = 0.011$, 77 deg nacelle angle

110 knots, $C_T = 0.008$, 60 deg nacelle angle

Figure 10. DCP measurements for various speeds in level flight. $^{X}/_{D} = 2.818$

large, positive DCP indicated in Fig. 9(a).

Continuing outboard, recall the region of negative DCP just outboard of three semispans. With the trail aircraft in this position, the right rotor has moved completely free from the lead aircraft wake. The left rotor, however, will continue to experience upwash from the wake super vortex at $^{Y}/_{s} = 1.6$. This upwash, acting solely on the left rotor produces a small positive roll moment that is balanced by low negative DCP.

The detailed velocity measurements of the PIV technique permit a quantitative analysis of the trail aircraft aerodynamic environment. When the trail aircraft is positioned at the point of maximum DCP, the PIV plane intersects the rotor disks along a line that passes through the "$\times$" in Fig. 9(a) and extends from approximately $^{Y}/_{s} = 0.2$ to $^{Y}/_{s} = 3.8$. The three velocity components measured along this line can be combined and resolved into upwash and edgewise components relative to the trail aircraft rotors (Fig. 9(c)). The result is presented in Fig. 9(d). The ordinates in this plot are now the velocity perturbations measured at the trail aircraft rotor disks, normalized by V_h. The gray boxes in Fig. 9(d) represent the regions along the abscissa occupied by the rotors of the trail aircraft.

From Fig. 9(d), it is clear that there is very little change in the in-plane components of velocity, labeled "Edgewise", except where the outboard tip of the left rotor enters the model support strut wake. Additional testing has indicated that these small, highly-localized velocity deficits originating from the support strut do not result in significant roll moments on the trail aircraft. Rather, the genesis of the counterclockwise roll moment at this location is readily observed in the out-of-plane velocity components—those labeled "Upwash". From the blue curve in Fig. 9(d), it is clear that while the right rotor experiences relatively unperturbed flow, the left rotor experiences significant downwash across most of the disk. This downwash reduces the thrust of the left rotor, thereby generating a negative roll moment on the trail aircraft.

The Effect of Speed in Level Flight

Of the independent variables considered for these tests, one of the most conspicuous is flight speed. Figure 10 gives DCP survey results as a function of flight speed. From Fig. 10, it is clear that the influence of the lead aircraft varies significantly with flight speed. At 20 knots, the peak DCP is two degrees and nearly all of the survey plane indicates some positive DCP required

of the trail aircraft. At 50 knots, the peak DCP required is undiminished, but the region requiring positive DCP is smaller. Also, a region of negative DCP begins to appear near $Y/s = 4$. Above 50 knots, peak DCP—both positive and negative—falls off quickly. However, the contour shapes and sizes change little.

Also worth noting is the location of peak DCP. At 20 knots, peak DCP occurs at $Y/s = 3.1$ and $Z/s = -3$. At 50 knots, the DCP peak climbs to $Z/s = -0.5$ and moves inboard approximately one semispan where it remains as speed continues to increase.

Figure 11 shows PIV measurements acquired at these same conditions. At 20 knots, the wake is dominated by regions of out-of-plane velocity perturbation, with little out-of-plane vorticity. Examining velocities in the rotor plane of the trail aircraft reveals that roll moment is the result of differences in both edgewise and upwash components of velocity. A slight upwash over the whole right rotor produces a small increase in thrust on that rotor. In addition, much of the left rotor experiences downwash which acts to reduce the thrust on that rotor. These phenomena combine to produce a negative roll moment on the trail aircraft. A similar trend can be witnessed in the edgewise component of velocity. A small increase in edgewise velocity on the right rotor increases the advance ratio—and hence the thrust—of this rotor. This is paired with a small decrease in edgewise velocity on the left rotor—causing a similar decrease in thrust—to also produce a negative roll moment.

At a flight speed of 50 knots, the out-of-plane velocity distortions are greatly diminished spatially, and a powerful vortex forms at $Y/s = 2$. The most significant contribution to roll moment comes from asymmetric inflow generated by this super vortex: upwash over the entire right rotor and downwash over the entire left rotor result in a negative roll moment. The edgewise component of velocity features a small, negative-roll-inducing deficit over much of the left rotor. The most significant feature of the edgewise velocity distribution, a hump centered between the two rotors, affects the left and right rotors equally and does not induce any roll on the trail aircraft.

The prominent velocity deficit near $Y/s = 6$ for speeds of 50 knots and above in Fig. 11 is non-physical—the result of a shadow cast on the PIV laser light sheet.

At 80 knots, the character of the PIV measurements changes little. The wake super vortex continues to generate roll moment through upwash and downwash along the span of the trail aircraft. Note that as speed increases, the super vortex moves inboard and becomes slightly more concentrated.

At 110 knots, the trail aircraft right rotor sees little disturbance whereas the left rotor experiences both upwash and downwash due to the super vortex. Mutual cancellation between these regions of upwash and downwash partially explains the reduction in peak DCP at this speed.

Note also the region of increased out-of-plane velocity near the super vortex at 110 knots. This is likely generated by the rotor disk which was tilted forward 25 deg compared to the 50 knot case. This nacelle tilt would direct an increased portion of the rotor wake energy in the streamwise direction. The highly perturbed streamwise flow results in an interesting distribution of edgewise velocity on the left rotor of the trail aircraft. Notice that the outboard half of the left rotor—the advancing side—encounters a velocity deficit whereas the retreating side of the left rotor encounters a velocity surplus. On either side of the rotor disk, the result is reduced flow speed seen by individual blades. Therefore, this inboard velocity surplus results in a greater loss of rotor thrust than would occur if the entire rotor experienced edgewise velocity deficit.

The reduction in peak DCP required of the trail aircraft at speeds above 50 knots may have origins in the trail aircraft itself. Careful examination of Fig. 10 reveals that the rotor thrust coefficient decreases steadily as speed increases. This is the result of increasing lift from the tiltrotor airframe partially unloading the rotors. In addition, the nacelles tilt forward as speed increases. This nacelle tilt reduces the component of rotor thrust that contributes to aircraft roll. Because of the rotor unloading and nacelle tilt, the component of rotor thrust that can generate roll on the trail aircraft at 110 knots is just 49% of the of the roll-inducing thrust at 20 knots. Perturbations to rotor thrust due to the lead aircraft wake at 110 knots are expected to have a similarly reduced effect on trail aircraft roll moment.

Observe that at all speeds, the location of peak DCP remains very close to the super vortex. The causal relationship between the super vortex, upwash, and peak DCP demands this coupling, and explains the variation in position of peak DCP observed in Fig. 10.

For the rest of this paper, 50 knots will be used as a baseline for comparison. Below 50 knots, the region of peak DCP is pushed far below the lead aircraft. It is unlikely that a trail aircraft would operate in this region in the course of normal operations. Above 50 knots, the interaction between the two aircraft is alleviated. A flight speed of 50 knots can therefore be considered a worst case for normal operations.

The Effect of Climb/Descent Rate

Other important flight conditions considered for this study included climbing and descending flight. First, consider flight at a constant descent angle as shown in Fig. 12. In this figure, the formation flight path angle, γ, is fixed at -11.4 deg. As speed was increased, descent rate was similarly increased to hold this angle constant.

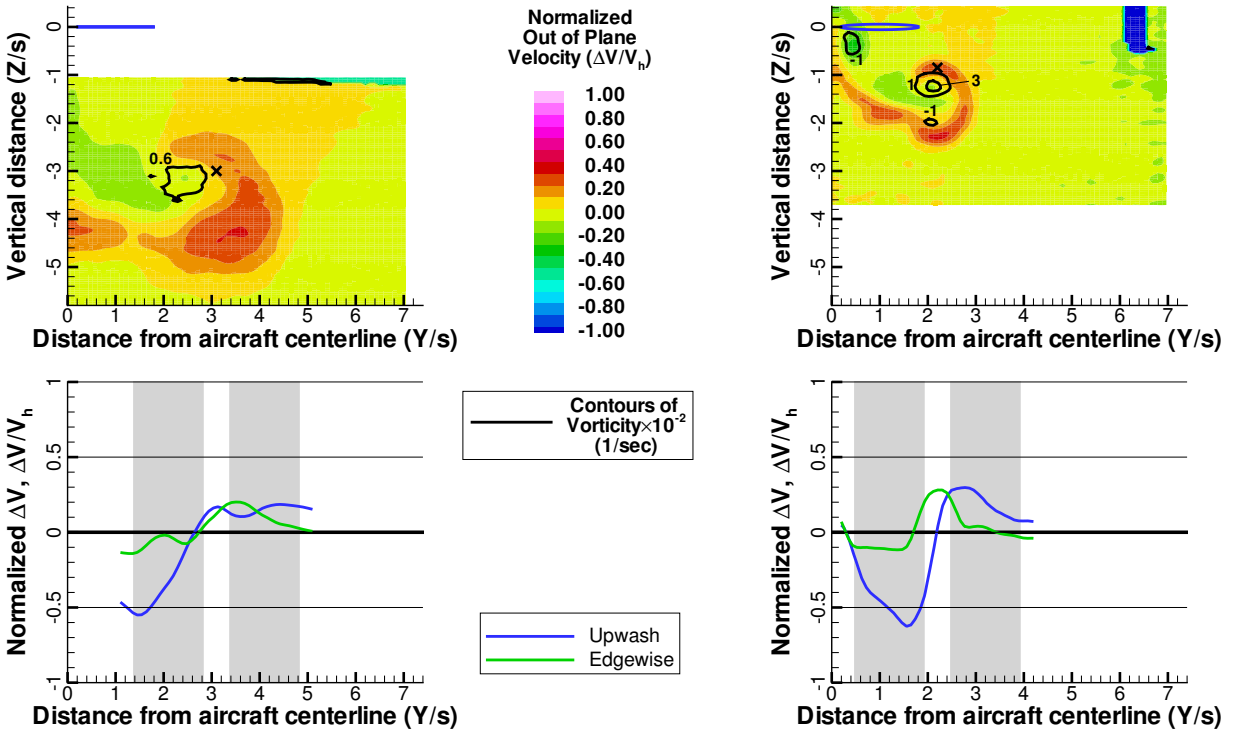

20 knots, $C_T = 0.014$, 90 deg nacelle angle

50 knots, $C_T = 0.013$, 85 deg nacelle angle

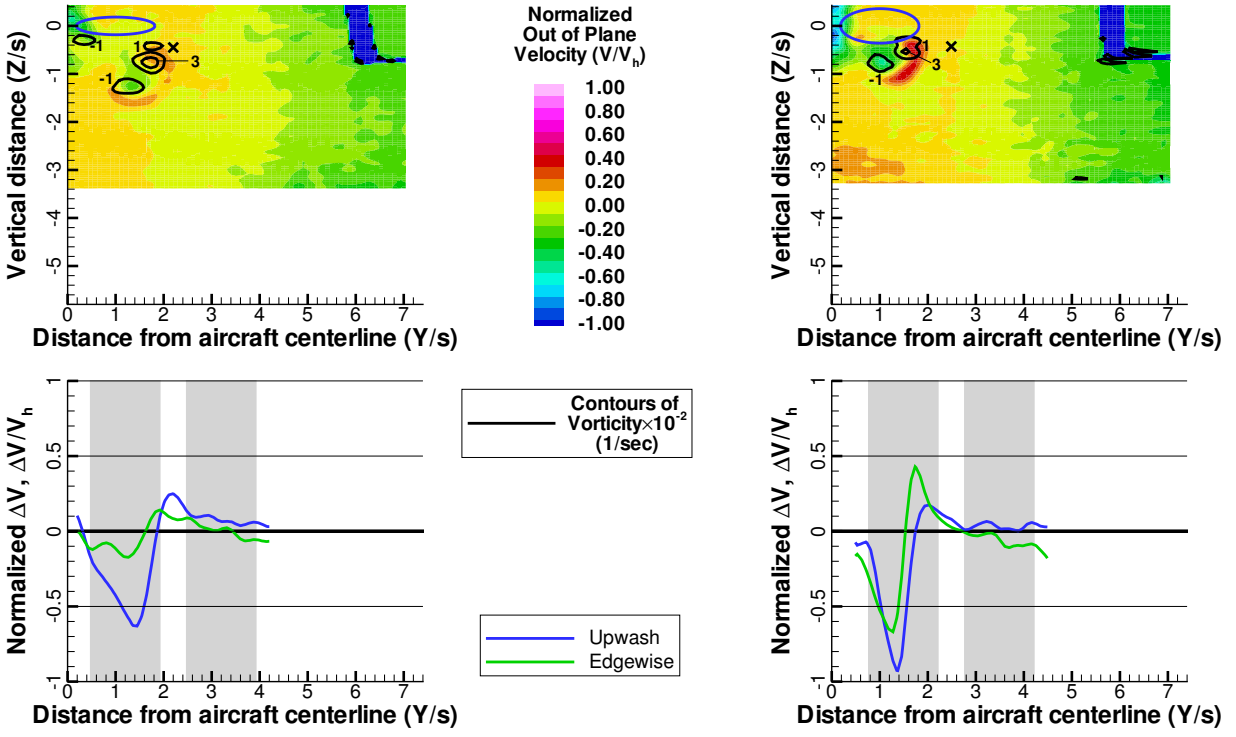

80 knots, $C_T = 0.011$, 75 deg nacelle angle

110 knots, $C_T = 0.008$, 60 deg nacelle angle

Figure 11. PIV measurements for various flight speeds. Level flight. $^{X}/_{D} = 2.818$

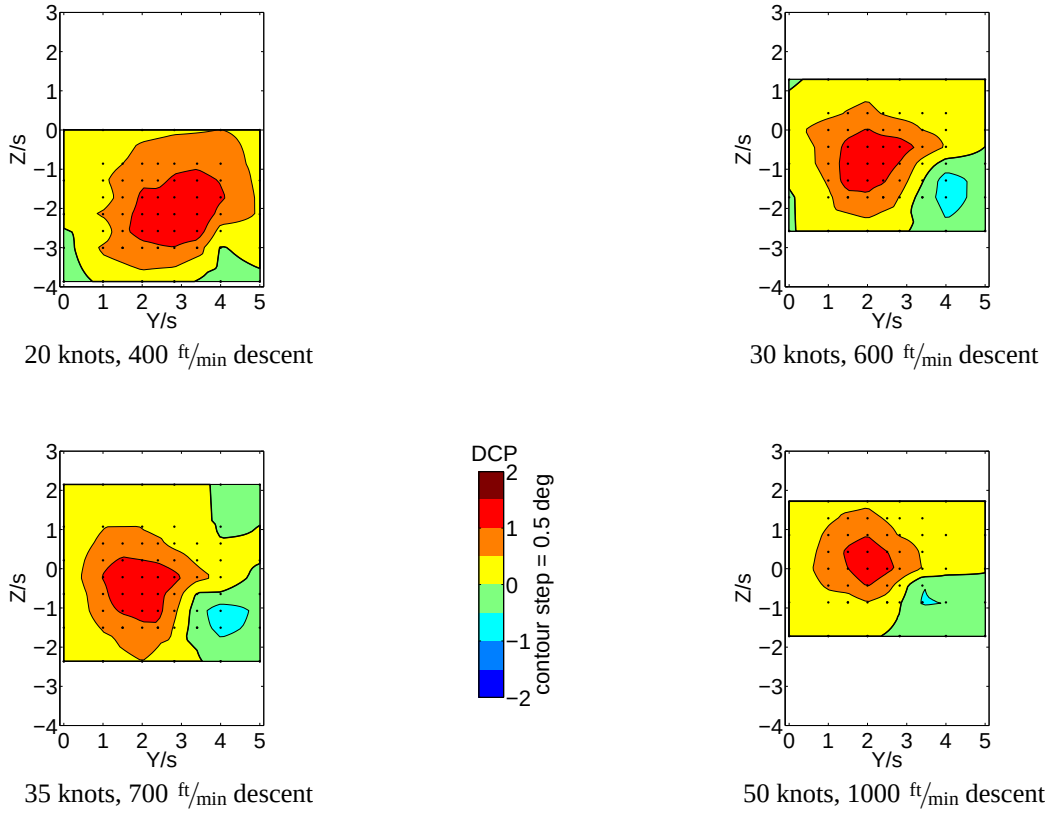

Figure 12. Contours of DCP for formation flight at various speeds with a constant descent angle of $\gamma = -11.4$ deg. $x/D = 2.818$, $C_T = 0.014$

Not surprisingly, the trend witnessed in Fig. 12 is similar to Fig. 10 in which speed was varied in level flight. As speed and descent rate are increased in Fig. 12, the peak DCP required of the trail aircraft changes little, but the regions of positive DCP become more compact. However, whereas the peak DCP at 20 and 50 knots is 2 deg in level flight (Fig. 10), it is just 1.5 deg in Fig. 12. The effect of decreasing the flight path angle appears to have been to reduce the peak DCP.

Figure 13 presents changes in trail aircraft DCP for a formation in which flight speed is held constant while the flight path angle is allowed to vary. The three surveys at the top of Fig. 13 exhibit the interaction between aircraft for formations in climb or level flight. Compared to level flight, positive flight path angles (climbing flight) experience little change in the peak DCP required of the trail aircraft. The peak DCP contour—and this contour alone—does appear to have expanded slightly in the climbing configurations. The descending flight cases in Fig. 13 clearly indicate a reduction in peak DCP as descent rate increases. At the steepest descent rate of 2500 ft/min, regions of significant interaction ($|\text{DCP}| > 0.5$ deg) appear to be vanishing.

Notice also that there is a gradual shift in the location of the negative and positive peak DCP contours. In climbing and level flight, the negative contour is located beside the peak positive contour. At moderate descent rates, the negative contour appears to move downward relative to the positive contours. At the highest descent rates, the positive contour shifts outboard while the negative contour shifts inboard.

Lastly, observe the vertical shift in the location of peak positive DCP that occurs at each new descent rate. As the formation flight path angle decreases, the location of peak DCP rises steadily.

Figure 14 presents PIV measurements corresponding to three of the cases presented in Fig. 13. The character of the edgewise and upwash velocity distributions are by now familiar. In all three cases, downwash on the left rotor acts in unison with upwash on the right to induce negative roll moment on the trail aircraft. The roll-inducing effects of upwash are further enhanced by the edgewise velocity distribution which generally reduces the advance ratio on the left rotor while increasing it on the right.

The PIV measurement in climb has larger and more expansive out-of-plane velocity perturbations compared to the other descent rates. This may be responsible for the expanded peak DCP contour observed in Fig. 13.

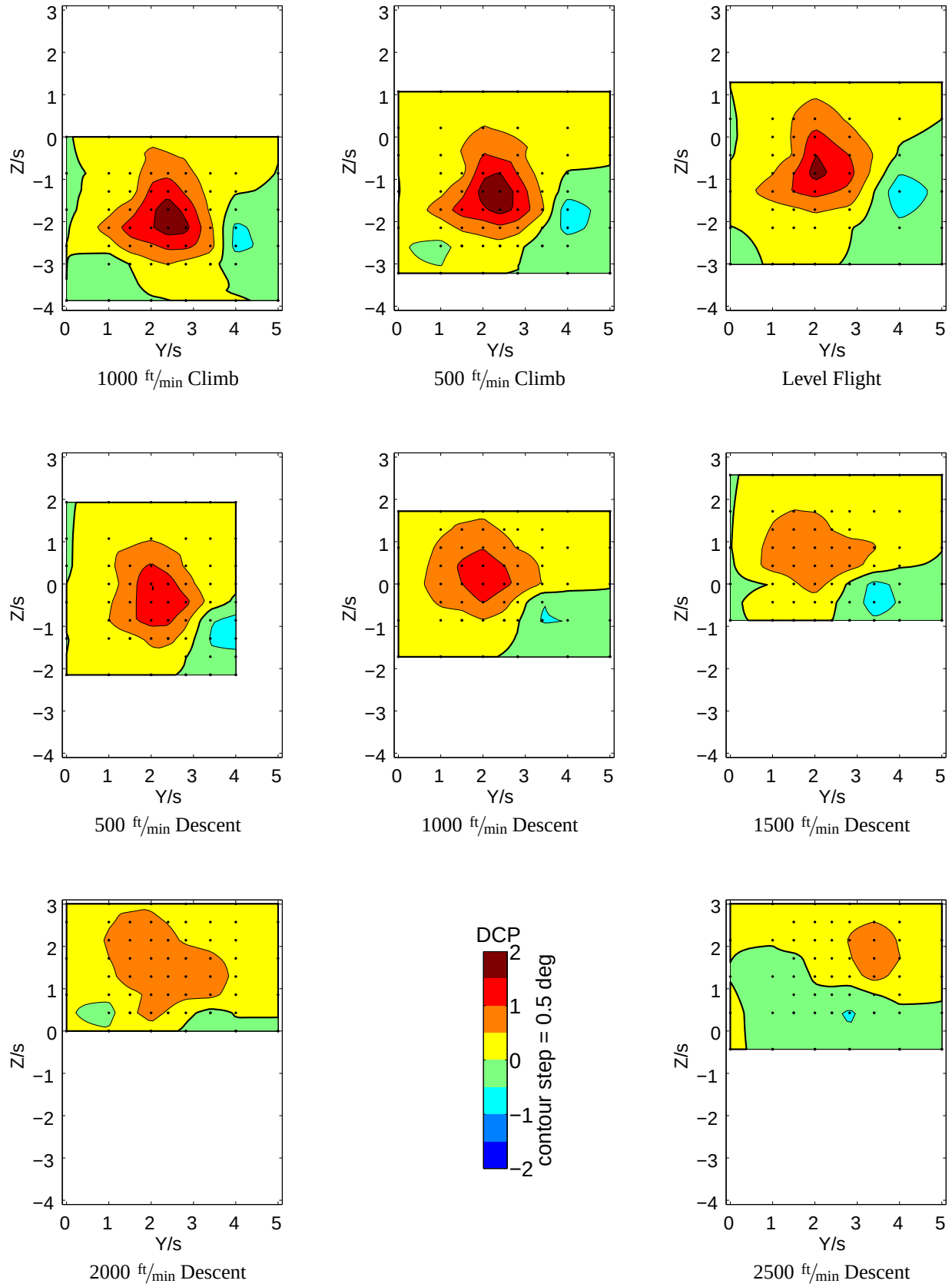

Figure 13. DCP required of trail aircraft at various rates of climb and descent. 50 knots, $C_T = 0.014$, $X/D = 2.818$

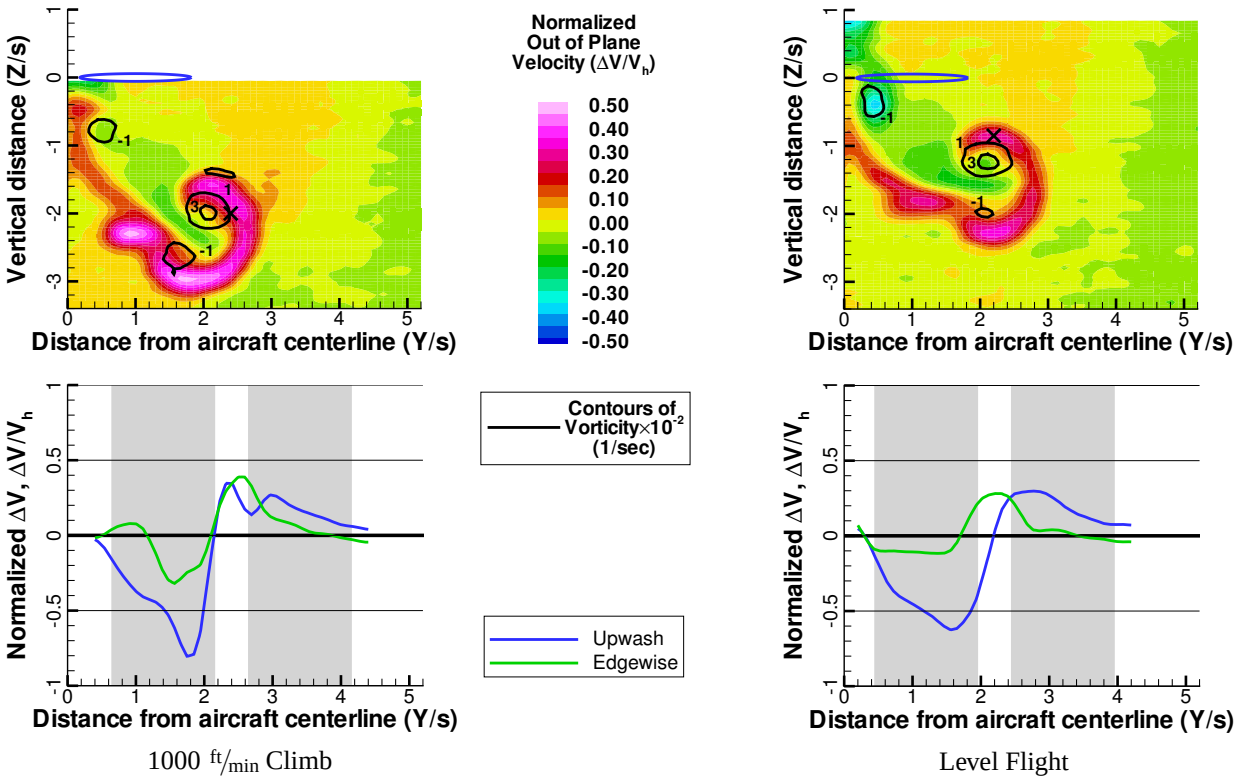

1000 $^{ft}/_{min}$ Climb

Level Flight

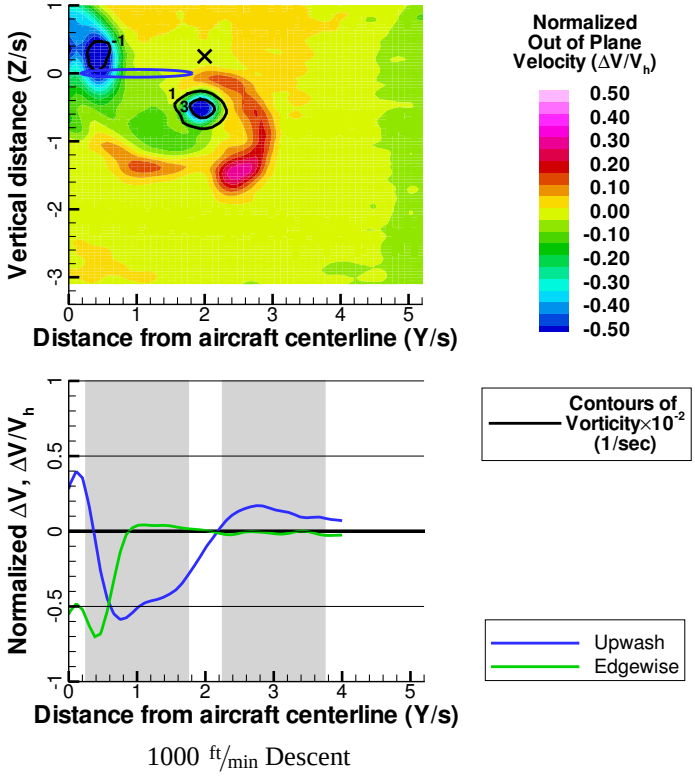

1000 $^{ft}/_{min}$ Descent

Figure 14. PIV measurements for various descent rates at 50 knots, $C_T = 0.014$, $^{X}/_{D} = 2.818$

Lacking PIV measurements at higher descent rates, it is not possible to extrapolate conclusions regarding the high descent rate trends witnessed in Fig. 13.

From Fig. 14, it is again clear that the location of peak DCP remains closely associated with the location of the super vortex. Changes in the vertical location of this vortex as descent rate varies explains the vertical shifts in the location of the peak DCP contour in Fig. 13.

The Effect of Longitudinal Separation

Because aircraft wakes dissipate over time, it is reasonable to expect the interaction between aircraft in a formation to diminish with increasing longitudinal separation. Unfortunately, Fig. 15 shows this dissipation is too slow to benefit aircraft separated by as much as nine rotor diameters. Figure 15(a) presents the interaction between the two aircraft for increasing longitudinal separation using a series of lateral survey planes. Figure 15(b) is a separate measurement of this interaction using a single longitudinal survey plane. This longitudinal survey plane is normal to the lateral planes and intersects the three closest planes at $^{Y}/_{s} = 2$. This longitudinal survey did not extend to $^{X}/_{D} = 9.0$.

Figure 15(b) clearly indicates that the peak DCP required of the trail aircraft persists far aft of the lead aircraft. It is not until the aircraft are separated by nine full rotor diameters (observable only in Fig. 15(a)) that the peak DCP subsides by a single contour step. Despite the reduction in peak DCP, the contour for $1 < \text{DCP} < 1.5$ deg does not change appreciably even at $^{X}/_{D} = 9$. Therefore, significant interaction exists as far aft as $^{X}/_{D} = 9$ even though the peak DCP has decreased. Notice that all of the DCP contours in Fig. 15(b) descend similarly to a rotor wake.

Figure 16 presents PIV measurements corresponding to the four lateral surveys in Fig. 15(a). Diffusion of the wake is evident as separation between the aircraft increases. The out-of-plane velocity perturbations quickly disperse into a region of mildly accelerated flow that seems to rotate about the wake super vortex. In addition, the peak vorticity of the super vortex for the two closest formations is 0.03/sec. At larger separations, this vorticity decreases to just 0.01/sec. This reduction in vorticity is indicative of either vortex diffusion or vortex decay. In either case, the result is reduced in-plane velocity in the vicinity of the super vortex.

Changes in the wake super vortex are evident in the reduced downwash into the trail aircraft rotors as formation separation increases. The point of maximum DCP also strays further from the super vortex core with increasing distance between aircraft. Both of these facts suggest that the wake super vortex plays a diminished role in inducing roll on the trail aircraft as formation separation increases.

Increasing aircraft separation has little effect on edgewise velocity at the trail aircraft rotor disks. All four PIV measurements indicate similar negative roll tendency due to edgewise velocity perturbation.

The Effect of Sideslip

The effect of varying formation sideslip on trail aircraft DCP can be seen in Fig. 17. If a formation flying at 50 knots enters a -15 deg sideslip, the peak DCP increases from 1.7 deg to 2.2 deg and shifts outboard approximately 1.5 semispans. The outboard shift of peak DCP is also present for a formation flying at 20 knots. However, the magnitude of peak DCP behaves very differently in that it *decreases* from 1.7 deg to 1.5 deg with sideslip.

Reviewing Fig. 3, bearing in mind that the aircraft wake convects in the wind axis and not in the inertial axis, it is easy to understand why the location of peak DCP moves outboard as sideslip increases. With no sideslip, the wake convects parallel to the X-Z plane, but non-zero sideslip causes the wake to convect diagonally, out of this plane. The force and moment survey plane is rooted in the inertial axis system and experiences the diagonal wake convection as a lateral shift. Considering this geometry, the expected shift is:

$$\frac{\Delta Y}{s} = \frac{X}{D} \cdot \frac{D}{s} \cdot \tan\beta = 1.23$$

This is in good agreement with the shift observed in Fig. 17.

The trend in peak DCP magnitude with flight speed and sideslip angle is not easily explained. The trend is inconsistent across speeds, decreasing with sideslip at 20 knots yet increasing with sideslip at 50 knots. Lack of additional information makes it difficult to determine the phenomena at work.

The Effect of Rotor Thrust

Wake vortices are a primary factor in determining the difficulty that the trail aircraft will have maintaining steady flight. A strong vortex will generate more upwash—and therefore more roll moment—on an aircraft than a weaker vortex in the same position. The strength of wake vortices encountered by a trail aircraft is determined by the disk loading of the lead aircraft. A heavy aircraft generates more thrust and thus stronger wake vortices.

Figure 18 illustrates the effect of lead aircraft gross weight on required DCP with a series of force and moment surveys. In this series of runs, the rotor thrust of the lead aircraft was set to represent various full-scale

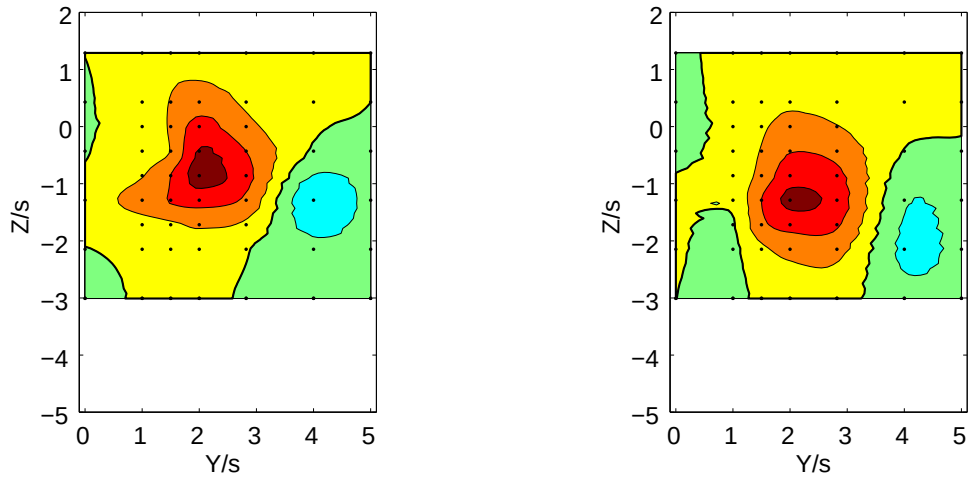

(a) Required DCP in Y-Z (lateral) survey planes

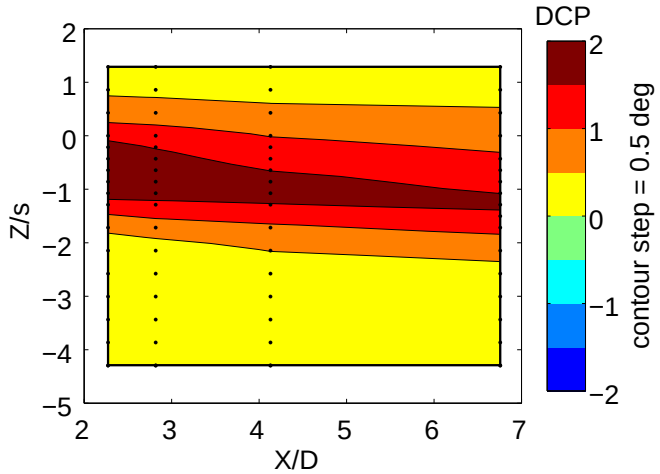

(b) Required DCP in an X-Z (longitudinal) survey plane at $Y/s = 2$

Figure 15. Trail aircraft DCP with increasing longitudinal separation. 50 knots, level flight, $C_T = 0.014$

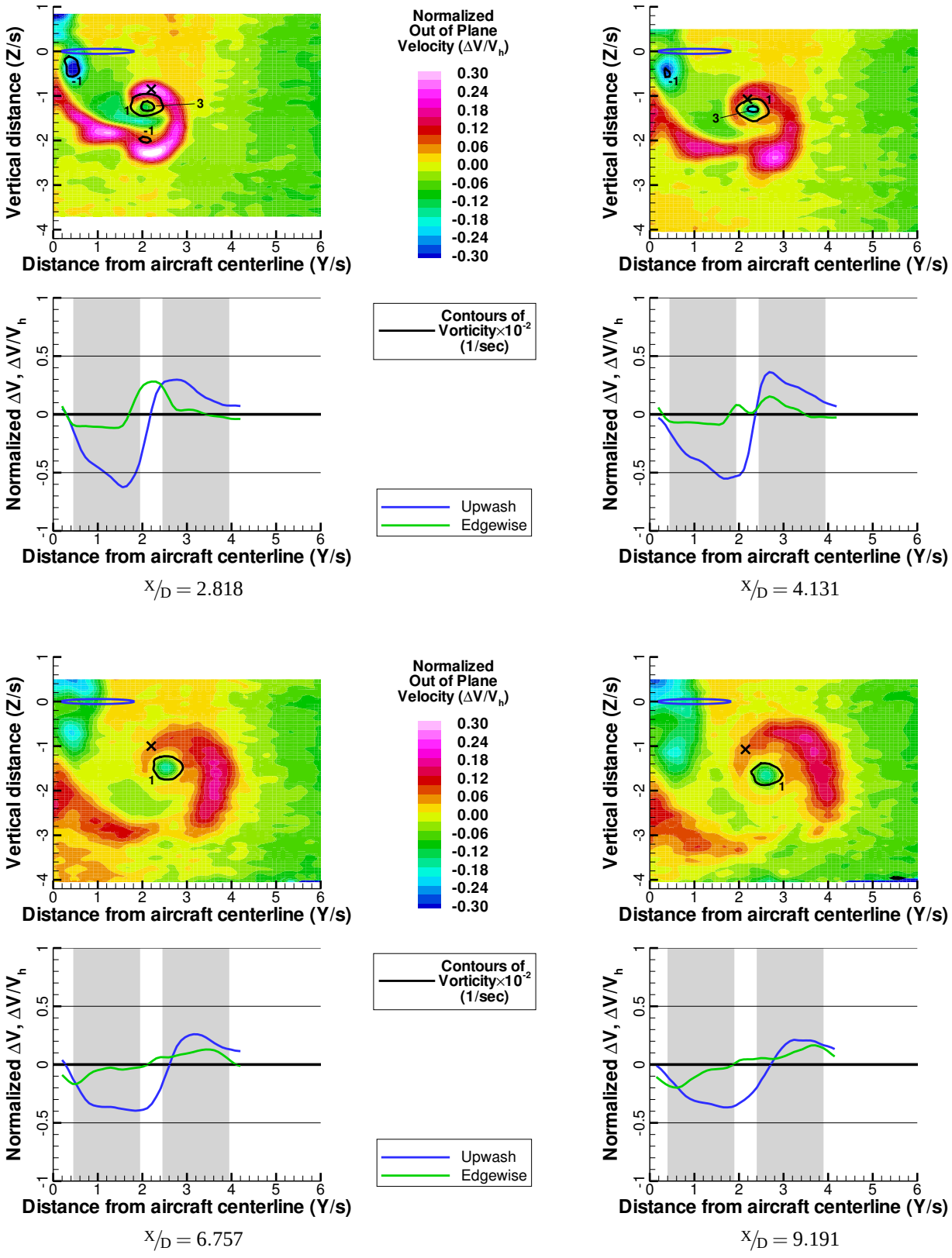

Figure 16. PIV measurements for various longitudinal separations. 50 knots, level flight, $C_T = 0.014$

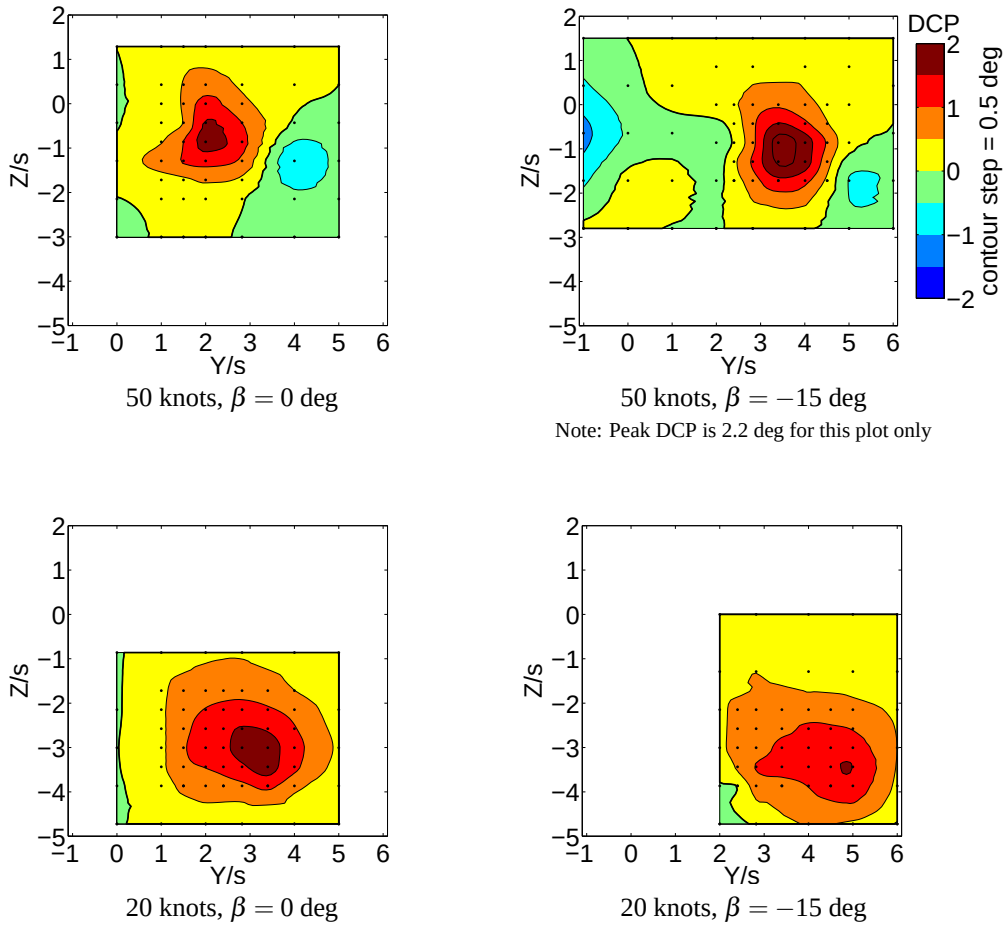

Figure 17. The effect of sideslip on trail aircraft DCP. 50 knots, level flight, $^{X}/_{D}$ = 2.818, C_T = 0.014

gross weights while the trail aircraft thrust was fixed at $C_T = 0.014$.

When the lead aircraft is at the high thrust condition, the peak DCP is slightly higher and the contour of peak DCP is enlarged as compared to the baseline $C_T = 0.014$. As expected, the converse is true when the lead aircraft gross weight and thrust are reduced.

Conclusions

The effort required of a trail aircraft to maintain stable flight in formation is a topic nearly as varied as the subject of rotorcraft wakes. The wake shed from the lead aircraft in a formation interacts with the trail aircraft in complex ways inducing widely varying forces and moments. There appear to be two wake components of significance when considering low-speed formation flight. First, the DCP required of the trail aircraft is influenced by wake vortices which cause differential inflow into the two rotors. Second, streamwise velocity perturbations can incur roll moment on the trail aircraft through differential advance ratio changes on the rotors.

The potential for the largest roll moments on the trail aircraft exists when the formation flight speed is 50 knots or below, the formation is in climb, or when the formation aircraft are operating at high gross weight. Less interaction occurs between aircraft in formation when the formation is descending or flying at speeds above 50 knots.

Longitudinal separation offers little remediation to the effects of wake interaction unless the aircraft are widely separated. Similarly, vertical separation is of fleeting value since the wake trajectory—and hence the vertical location of maximum DCP—vary directly with descent angle. Except when the formation is in sideslip, the lateral location of peak DCP is always positioned approximately one full wingspan to the left and right of the lead aircraft centerline. Because non-zero sideslip angle is a less common flight condition than variation in flight path angle, formations that laterally offset the trail aircraft by more than one wingspan are recommended as the most effective means of wake avoidance.

In the course of these tests, the maximum DCP that

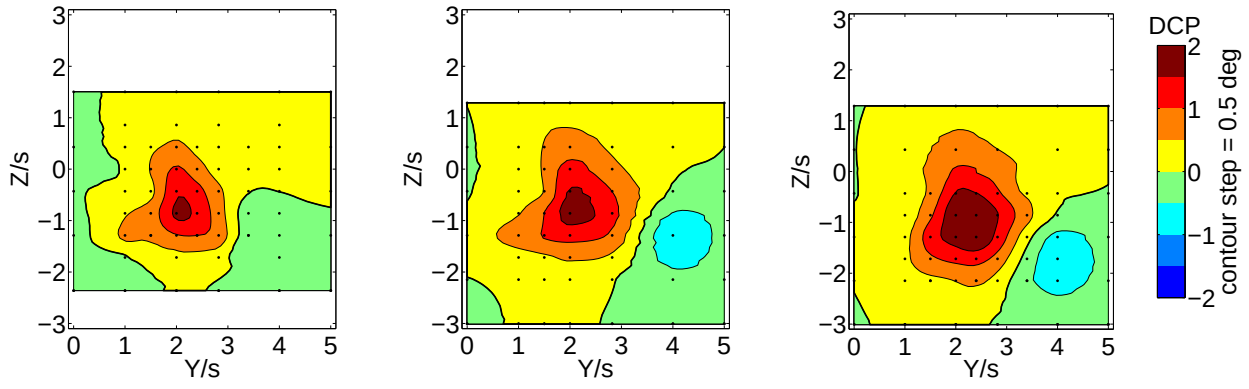

Figure 18. DCP contours resulting from variations in lead aircraft gross weight. 50 knots, level flight, $^{X}/_{D} = 2.818$

was required of the trail aircraft in any flight condition was 2.2 deg (see Fig. 17). This value occurred in level flight at 50 knots with -15 deg of sideslip. It is worth noting that the V-22 is capable of providing about 2.5 deg of DCP in most flight conditions. This roll control is further augmented by roll authority provided by the ailerons, especially at higher speeds. Therefore, the V-22 can operate safely in any of the tested conditions albeit with limited control margin at the worst locations.

References

1. Johnson, W., Yamauchi, G. K., Derby, M. R., and Wadcock, A. J., "Wind Tunnel Measurements and Calculations of Aerodynamic Interactions Between Tiltrotor Aircraft", AIAA-2003-47, American Institute of Aeronautics and Astronautics 41st Aerospace Sciences Meeting and Exhibit, Reno, NV, January 2003.

2. Yamauchi, G. K., Wadcock, A. J., and Derby, M. R., "Measured Aerodynamic Interaction of Two Tiltrotors", American Helicopter Society 59th Annual Forum, Phoenix, AZ, May 2003.

3. Silva, M. J., Yamauchi, G. K., Wadcock, A. J., and Long, K. R., "Wind Tunnel Investigation of the Aerodynamic Interactions Between Helicopters and Tiltrotors in a Shipboard Environment", American Helicopter Society 4th Decennial Specialist's Conference on Aeromechanics, San Francisco, CA, January 2004.

4. Rajagopalan, G., Niazi, S., Wadcock, A. J., Yamauchi, G. K., and Silva, M. J., "Experimental and Computational Study of the Interaction Between a Tandem-Rotor Helicopter and a Ship", American Helicopter Society 61st Annual Forum, Grapevine, TX, June 2005

5. Derby, M. R., and Yamauchi, G. K., "Design of 1/48th-Scale Models for Ship/Rotorcraft Interaction Studies", American Institute of Aeronautics and Astronautics 21st Applied Aerodynamics Conference, Orlando, FL, June 2003.